SINTEF
PROCEEDINGS
2

Proceedings of the 12th International Conference on Computational Fluid Dynamics in the Oil & Gas, Metallurgical and Process Industries

Progress in Applied CFD – CFD2017

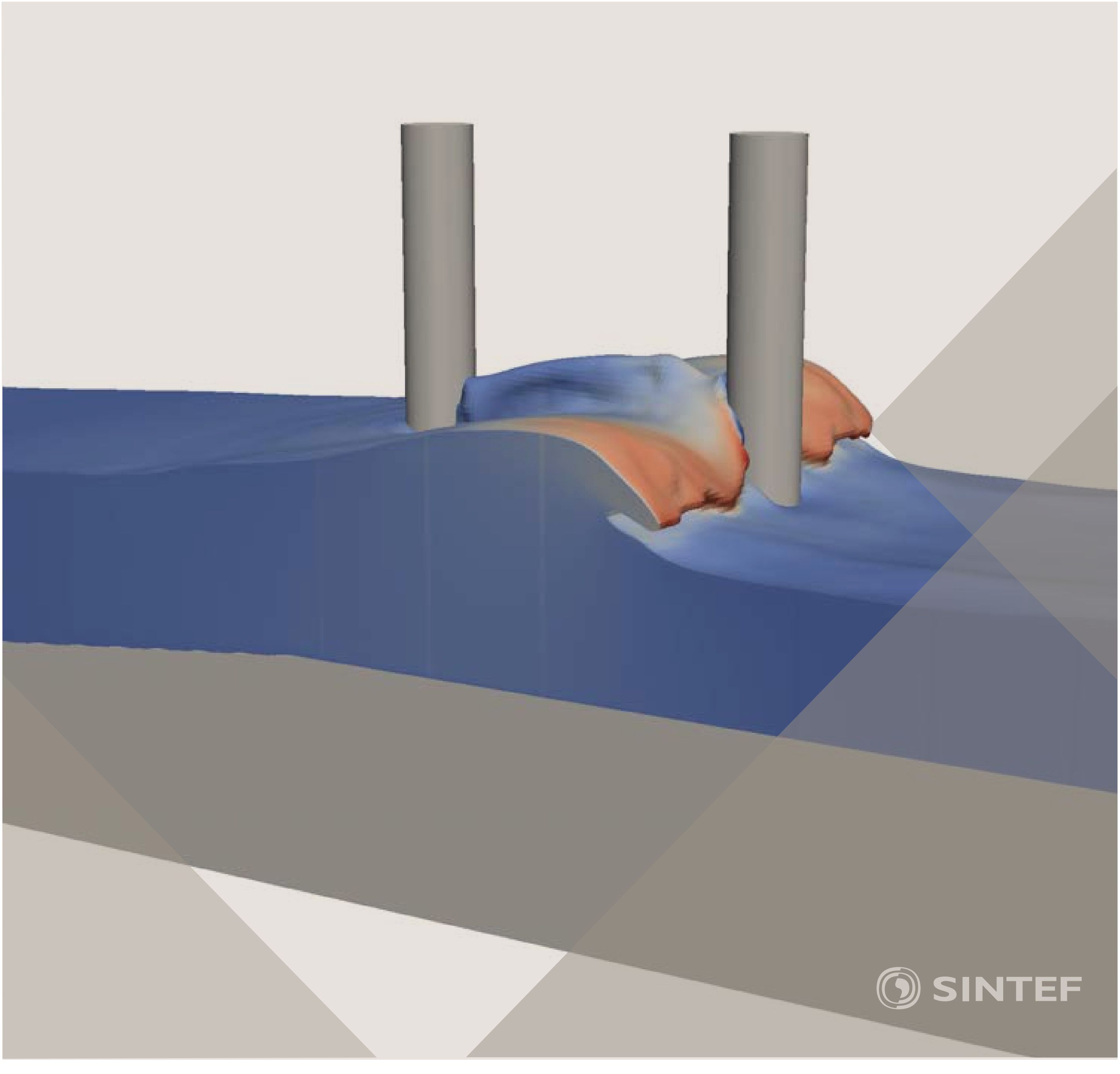

SINTEF

SINTEF Proceedings

Editors:
Jan Erik Olsen and Stein Tore Johansen

Progress in Applied CFD – CFD2017

Proceedings of the 12th International Conference on Computational Fluid Dynamics in the Oil & Gas, Metallurgical and Process Industries

SINTEF Academic Press

SINTEF Proceedings no 2
Editors: Jan Erik Olsen and Stein Tore Johansen

Progress in Applied CFD – CFD2017

Selected papers from 10th International Conference on Computational Fluid Dynamics in the Oil & Gas, Metallurgical and Process Industries

Key words:
CFD, Flow, Modelling

Cover, illustration: Arun Kamath

ISSN 2387-4295 (online)
ISBN 978-82-536-1544-8 (pdf)

SINTEF Academic Press

Address:	Forskningsveien 3 B
	PO Box 124 Blindern
	N-0314 OSLO
Tel:	+47 73 59 30 00
Fax:	+47 22 96 55 08

www.sintef.no/byggforsk
www.sintefbok.no

SINTEF Proceedings

SINTEF Proceedings is a serial publication for peer-reviewed conference proceedings on a variety of scientific topics.

The processes of peer-reviewing of papers published in SINTEF Proceedings are administered by the conference organizers and proceedings editors. Detailed procedures will vary according to custom and practice in each scientific community.

PREFACE

This book contains all manuscripts approved by the reviewers and the organizing committee of the 12th International Conference on Computational Fluid Dynamics in the Oil & Gas, Metallurgical and Process Industries. The conference was hosted by SINTEF in Trondheim in May/June 2017 and is also known as CFD2017 for short. The conference series was initiated by CSIRO and Phil Schwarz in 1997. So far the conference has been alternating between CSIRO in Melbourne and SINTEF in Trondheim. The conferences focuses on the application of CFD in the oil and gas industries, metal production, mineral processing, power generation, chemicals and other process industries. In addition pragmatic modelling concepts and bio-mechanical applications have become an important part of the conference. The papers in this book demonstrate the current progress in applied CFD.

The conference papers undergo a review process involving two experts. Only papers accepted by the reviewers are included in the proceedings. 108 contributions were presented at the conference together with six keynote presentations. A majority of these contributions are presented by their manuscript in this collection (a few were granted to present without an accompanying manuscript).

The organizing committee would like to thank everyone who has helped with review of manuscripts, all those who helped to promote the conference and all authors who have submitted scientific contributions. We are also grateful for the support from the conference sponsors: ANSYS, SFI Metal Production and NanoSim.

Stein Tore Johansen & Jan Erik Olsen

ANSYS®

metal production

NanoSim

Organizing committee:

Conference chairman: Prof. Stein Tore Johansen
Conference coordinator: Dr. Jan Erik Olsen
Dr. Bernhard Müller
Dr.Sigrid Karstad Dahl
Dr.Shahriar Amini
Dr.Ernst Meese
Dr.Josip Zoric
Dr.Jannike Solsvik
Dr.Peter Witt

Scientific committee:

Stein Tore Johansen, SINTEF/NTNU
Bernhard Müller, NTNU
Phil Schwarz, CSIRO
Akio Tomiyama, Kobe University
Hans Kuipers, Eindhoven University of Technology
Jinghai Li, Chinese Academy of Science
Markus Braun, Ansys
Simon Lo, CD-adapco
Patrick Segers, Universiteit Gent
Jiyuan Tu, RMIT
Jos Derksen, University of Aberdeen
Dmitry Eskin, Schlumberger-Doll Research
Pär Jönsson, KTH
Stefan Pirker, Johannes Kepler University
Josip Zoric, SINTEF

CONTENTS

VELOCITY PROFILES IN A 2D MODEL OF THE LEFT VENTRICULAR OUTFLOW TRACT, PATHOLOGICAL CASE STUDY USING PIV AND CFD MODELING

Paul R. LEINAN[1*], Paal SKJETNE[2†], John MORUD[2‡], Stig URHEIM[3§], Sigrid K. DAHL[2¶]

[1]SINTEF Petroleum AS, 7465 Trondheim, NORWAY

[2]SINTEF Materials and Chemistry, 7465 Trondheim, NORWAY

[3]Department of Heart Disease, Haukeland University Hospital, Bergen, Norway

* E-mail: paul.roger.leinan@sintef.no
† E-mail: paal.skjetne@sintef.no
‡ E-mail: john.c.morud@sintef.no
§ E-mail: stig.urheim@gmail.com
¶ E-mail: sigrid.dahl@sintef.no

ABSTRACT

In the current study, we present an experimental (in vitro) 2D flow model for studying blood flow in the human left ventricular outflow tract (LVOT) and the first part of the aorta using particle image velocimetry (PIV) and computational fluid dynamics (CFD). Two cardiac pathologies were investigated in this study; 1) anterior mitral leaflet (AML) billowing, and 2) asymmetric septal hypertrophy (ASH). Each of these conditions has the potential to alter the normal direction of the flow entering the aortic valve apparatus from the LVOT and therefore place an abnormal stress distribution on the aortic valve leaflets. We found good agreement between the PIV results and the CFD calculations. The largest discrepancy between the experimental data and the numerical results was found in the recirculation zone adjacent to the left coronary leaflet. The main limitations in the current study when evaluating the clinical significance of the results are the choice of a 2D geometry with stiff and stationary walls. Keeping this in mind, our results show that AML billowing and ASH bulging alone does not alter the flow field in the LVOT dramatically. However, when the two conditions combine, we see a significant flow separation and re-circulation zone forming at the left coronary leaflet, covering half of the aortic outflow tract at peak systole.

Keywords: In-vitro, PIV, CFD, Left ventricle.

NOMENCLATURE

Greek Symbols
ρ Mass density, [kg/m^3]
μ Dynamic viscosity, [cP]
ψ Drag correction factor, [-]

Latin Symbols
p Pressure, [Pa].
u Fluid velocity, [m/s].
d Diameter, [m].
Re Reynolds number, [-].
St Stokes number, [-].

Sub/superscripts
x Cartesian x component..
y Cartesian y component.
p Particle

INTRODUCTION

In the current study, we present an experimental (in vitro) 2D flow model for studying blood flow in the human left ventricular outflow tract (LVOT) and the first part of the aorta using particle image velocimetry (PIV), under both physiological and pathological conditions. The same setup was analyzed using computational fluid dynamics (CFD) and the results compared. Two cardiac pathologies were investigated in this study; 1) anterior mitral leaflet (AML) billowing, and 2) asymmetric septal hypertrophy (ASH). Each of these conditions has the potential to alter the direction of the flow entering the aortic valve apparatus from the LVOT and therefore alter the stress distribution on the aortic valve leaflets. In order to investigate the hemodynamic effects of AML billowing and ASH bulging on the aortic valve apparatus, the degree of AML billowing and ASH bulging was parametrized through parameters L1 and L2 in Figure 1.

There is a general agreements that the velocity profile in the LVOT and aortic annulus is flat but skewed, in previous Doppler ultrasound studies (at rest) (Sjöberg *et al.*, 1994; Kupari and Koskinen, 1993; Zhou *et al.*, 1993). Abnormal conditions such as AML and ASH which alters the geometry of the LVOT may have significant influence on the flow profiles in the same area (Matre *et al.*, 2003; Zhou *et al.*, 1993). However, previous studies on the hemodynamical influence of AML on LVOT are more scares in the literature, while some geometrical studies exists (Kvitting *et al.*, 2010). Some authors have used CDF models to study the hemodynamical effects of AML (Dahl *et al.*, 2011; Dimasi *et al.*, 2012; Xiong *et al.*, 2008), and reports that there is a non-negligible effect on the flow conditions in the aortic annulus due to AML billowing. In this work, we have build a simplified parametrized 2D model (both in an experimental lab setup and CFD) of the LVOT and aortic annulus were we can test hypotheses regarding the hemodynamical effects of AML billowing and ASH on the velocity profile in the aortic annulus and the load on the aortic vale leaflets. With this model setup, we also believe that we will be better equipped to point out directions where more detailed studies are needed, e.g. with 3D CFD and fluid-structure simulation models as well as 3D Doppler and 4D MRI studies of blood flow in the LVOT.

The two main limitations in our choice of model setup are; 1) the flow field is 2D, which may introduce unnatural flow conditions compared to the real 3D case, such as increased vortex formation, and 2) the walls are non-deformable and stationary. However, our model offers very good visual and

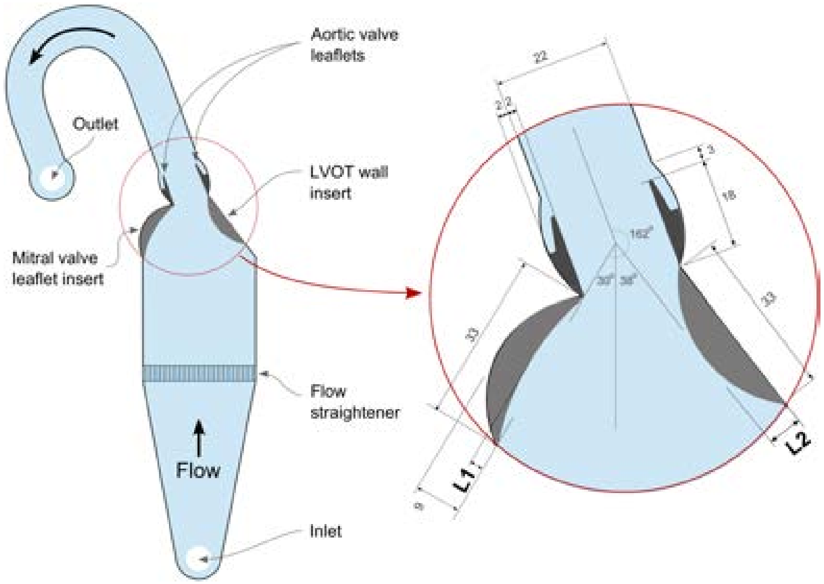

Figure 1: The flow domain geometry (blue area) which is cut into a 10mm thick Plexiglass plate by a water jet. A 40/60% glycerol-water mixture enters the model through the "inlet" port, then flows through the "flow straightener" before entering the LVOT and the aortic valve apparatus, finally the flow follows the aortic arc and exits through the "outlet". The degree of AML billowing and ASH are parametrized with Plexiglass inserts with different widths defined by the lengths L1 and L2.

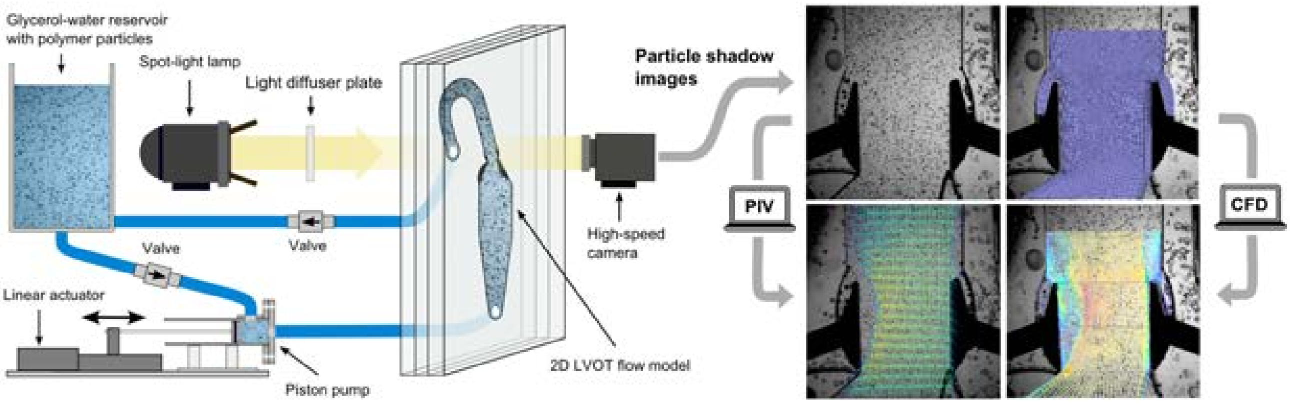

Figure 2: Illustration of the experimental setup, which consists of a fluid reservoir, the 2D LVOT flow model, a piston pump, a linear actuator (Zaber, X-LRQ-E) and connecting fiber reinforced 1" tubes and one-way polymer ball valves (SXE PVC-U, 1"). Fluid can be pumped through the loop and the LVOT model a pulsatile manner, determined by the waveform given to the linear actuator. The flow field in the 2D LVOT model was visualized by tracking the movement of polymer particles by recoding their shadows projection with a high-speed camera (Photron, FASTCAM 1024 PCI). The particle shadows where projected into the camera from a spot-light lamp (dedolight DLH400DT) and a light diffuser plate inline with a the camera.

quantifiable access to the LVOT flow field. Our geometry was based on conditions at peak systole when aortic leaflets are fully open, we will therefore focus our measurements on this period of the cardiac cycle. At the onset of the systole the aortic valve opens fully in typically less than 30 ms.

METHODS

Experimental setup

The LVOT flow model consists of three Plexiglass plates. The geometry of the flow domain, seen in Figure 1, was cut out of the middle plate by a water jet. This plate was then sandwiched between the two uncut Plexiglas's plates, as illustrated in Figure 2. In this way, the 2D flow domain was sealed inside the plates providing excellent visual access to the flow field. The middle plate was 10mm thick. Flow inlet and outlet ports were mounted on the uncut plates. The LVOT geometry is extracted from ultrasound recording provided by Dahl (2012) at peak systole, and is given by the so-called long axis view from such recordings defined as the 2D plane through the center of the aortic valve annulus, the mitral valve annulus and the apex of the left ventricle.

A flow loop was built so that fluid could be circulated through the LVOT model in a pulsatile manner. The flow loop is illustrated in Figure 2, and is made up of; the 2D LVOT flow model, a fluid reservoir, a piston pump and connecting tubes and one-way valves. The piston pump was connected to a programmable linear actuator (Zaber, X-LRQ-E) so that an an arbitrary flow pulse could be injected into the model in displacement control. Two ball valves (SXE PVC-U, 1") and fiber reinforced 1" transparent PVC tubing connected the loop components and ensured that unidirectional pulsatile flow could be circulated through the flow loop setup.

The blood analog fluid consisted of 60% deionized water and 40% Glycerol, which at room temperature gives a Newtonian fluid with a dynamic viscosity of $\mu = 3.6$mPa.s (Yousif *et al.*, 2011).

The velocity field in the 2D plane of the LVOT model (i.e. the flow domain described by Figure 1) was quantified by particle image velocimetry (PIV). In our case we added polymer particles to the reservoir tank, which were circulated in the loop, hence there was a uniform concentration of particles in the system. The particles were visualized by spotlight lamp (dedolight DLH400DT) inline with a light diffuser plate, the 2D LVOT flow domain and a high-speed camera (Photron, FASTCAM 1024 PCI), as seen in Figure 2. In this setup the shadows of the particles could clearly be seen in the flow domain on a white background because of the light diffuser plate. However, the quality of the visualization depended on several factors such as the distance between the spot-light lamp, the diffuser and the flow domain, the polymer particle size and the high-speed camera resolution (other important factors where also particle concentration, light intensity, camera shutter speed and aperture). The particle size compared to the camera resolution was particularity important, i.e. the size of the shadow needed to be larger than the size of the image pixels. In our current setup with the necessary zoom and a camera resolution of 512x512 (needed in order to have a frame rate of 3000 frames/sec), we achieved a pixel resolution of 0.013 pixels/μm. Hence, we used 80 μm polymer particles (Dynoseeds®TS 80), having a density of 1050 kg/m^3. According to Tropea *et al.* (2007) tracing accuracy errors for spherical traces are below 1% if the Stokes number is significantly smaller than 0.1. Stokes number with Reynolds number drag correction (Israel and Rosner, 1982) may be given by

$$St = \frac{\rho_p d_p u}{18\mu}\psi(\mathrm{Re}_d) \qquad (1)$$

where ρ_p and d_p are the particle density and diameter, respectively, and $\psi(\mathrm{Re}_d)$ is the drag correction factor. In the current setup flow velocities around 1.0 m/s are expected in the LVOT, which by Eq. 1 gives a Stokes number of $St \approx 0.75$.

The recorded shadow particle images were post processed using the open source software OpenPIV (python version, 0.20.5) (Taylor *et al.*, 2010). Default settings in the software was used during PIV calculations with a window size of 24 and overlap of 20 pixels.

Experimental protocol

The two pathologies investigated in this study can be seen in Figure 1, defined by the parameters L1 and L2. L1 defines the degree of AML billowing and L2 defines the degree of ASH. Four cases were studies in the current work, as given in Table 1 the normal physiological geometry, case 1; AML billowing, case 2; ASH, case 3; and a combination of AML billowing and ASH, case 4.

Table 1: Model parameter matrix with; the normal physiological geometry, case 1; AML billowing, case 2; ASH ,case 3; and a combination of AML billowing and ASH, case 4, as depicted in Figure 1

	AML	ASH
Case	L1 (mm)	L2 (mm)
1	0	0
2	0	9
3	9	0
4	9	9

The experiments started with preparing the 40/60% glycerol-water mixture which was added to the reservoir tank, as seen in Figure 2. Polymer trace particles were then added (Dynoseeds®TS 80) until the particle density was sufficient to achieve good PIV quality. Care was taken to evacuate all air pockets and bubbles form the connecting tubes and vales, and the fluid mixture was circulated in the loop until a uniform distribution was obtained. The software controlling the inflow waveform (given by the linear actuator and the piston pump) was able to trigger the high-speed camera at a predetermined point in the cardiac cycle. Six full cardiac cycles were recorded with a frame rate of 3000 frames per second, for each of the four geometry cases in Table 1. The LVOT inflow waveform was obtained from ultrasound recording provided by Dahl (2012), defined by the volumetric change of the left ventricle during systole.

CFD model

The LVOT flow model described in the previous subsection was simulated using ANSYS Fluent 16.2. The computational domain was limited to the section after the flow straightener and the outlet was simplified to a simple in-plane rectangular outlet. The actual dimensions of the CFD domain and the flow loop were the same since the same underlying CAD was used to generate both the machined loop geometry and the CFD domain.

A hexahedral mesh was used, with a nominal grid resolution of 500 μm in the region of interest, i.e. the aortic root and lower part of the ascending aorta. A boundary layer was attached to the mitral and septal sides of the flow conduit with a starting size of 100 μm expanding with a factor of 1.2 in 9 layers. In the out of plane direction the resolution was 1 mm, and in the distal parts relative to the aortic root (inlet and outlet regions) the lateral resolution was decreased to 2 mm.

The flow is highly transient, the whole outflow lasting 360 ms. Thus, there is not enough time for steady state boundary layers to develop, and not time enough time for turbulence to develop. For these reasons we opt to use a laminar flow model, although at the aortic root the Reynolds number briefly rises to a value of approximately 6000 at peak systole (peak flow). The SIMPLE method was used for the pressure-velocity coupling, a second order upwind scheme for the momentum equation, a second order scheme for pressure, and gradient reconstruction was done using cell based least squares. A first order implicit formulation was used for the transient formulation. Estimated peak flow velocities are 1.5 m/s, and with a 100μm resolution this results in a time step requirement of 30 μs, we have employed a time step of 20 μs. Furthermore, constant density, 1050 kg/m^3, and Newtonian viscosity, 3.5 mPa.s, were employed.

At the outlet a pressure boundary condition was implemented, with zero gauge pressure, as the reference point for the pressure was also located at the center of the outlet. The inlet was modeled as a velocity inlet. The inlet velocity was determined in the following way: The volume curve obtained from a subject using ultrasound (Dahl, 2012) was used to give a physiological realistic time varying profile. This volume curve was converted into a time varying piston position, and the velocity was simply the derivative of this curve and is depicted in Figure 3. The inlet velocity was implemented using ANSYS Fluents user defined functions (UDF).

RESULTS

PIV and CFD results from the four LVOT geometry cases is presented in Figure 4. Additionally, the maximum axial velocities for the velocity profiles (blue solid lines) are given in

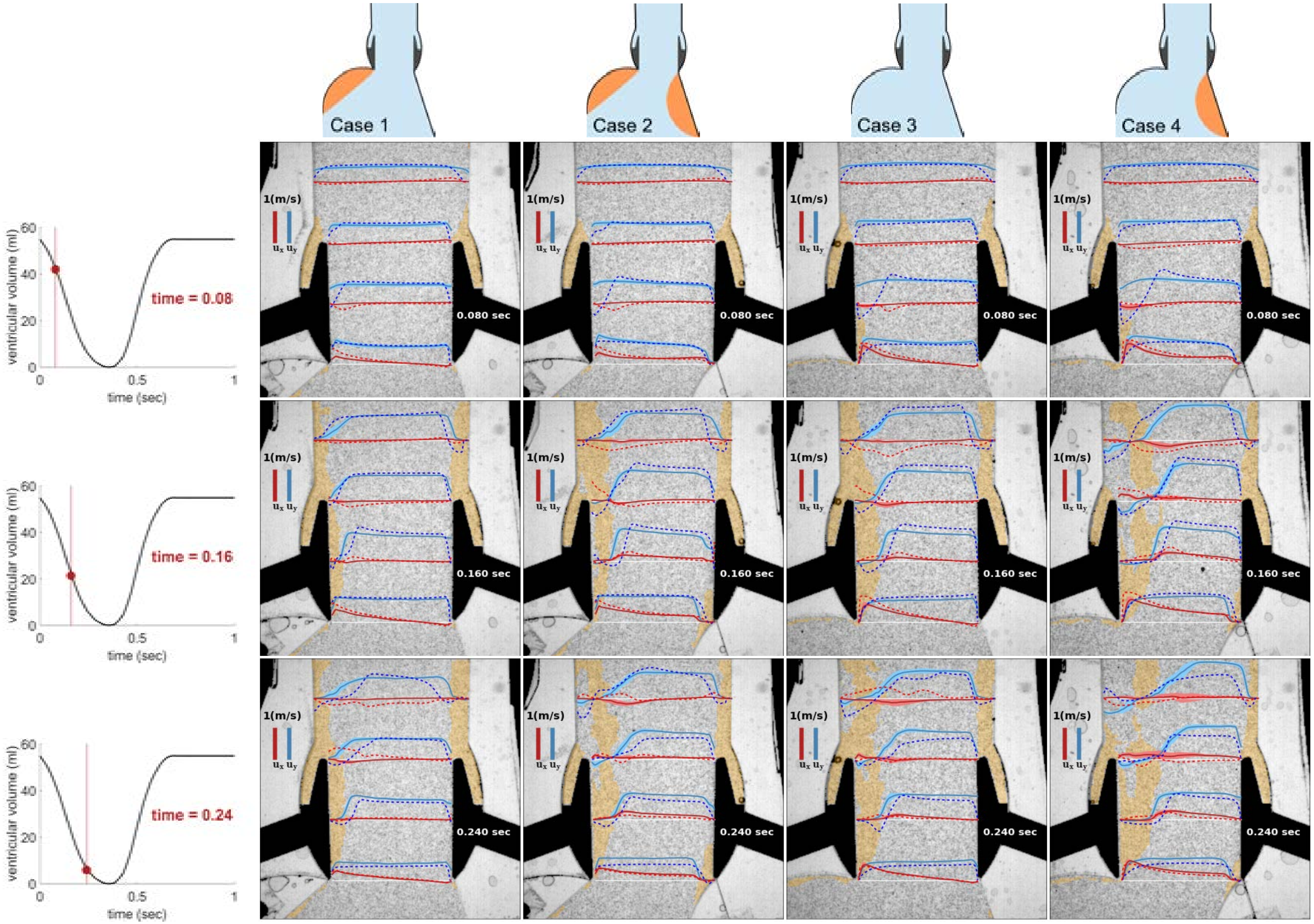

Figure 4: PIV and CFD results from the four LVOT geometry cases. The top row shows illustrations of the geometry of the LVOT for the four cases, where the inserts are colored orange. The inflow waveform used in the experiments is given in the left column from the top. The curves shows remaining ventricular ejection volume as a function of time which determines the volume flow in the loop. Systole begins at time zero and ends at 0.360 sec. Velocity profiles at three times during systole are given in the figure, at 0.08, 0.16 and 0.24 sec, respectively. The blue velocity profiles gives the velocity components in the axial direction (y-direction) and the red velocity profiles gives the velocity components in the transverse direction (x-direction). The PIV results from the in-vitro flow loop is given by solid lines, and is averaged from six cardiac cycles. Additionally, at the three selected times, velocities are averaged over a time span of 3 milliseconds. The plotted blue and red shaded areas give the standard deviation in the PIV data. The velocity profiles components from the CFD calculations are given by blue and read dashed lines, for the y and x direction respectively. The red and blue vertical bars in each figure gives the velocity profile scale of 1 m/s. Areas where the velocity magnitude is smaller that 0.1 m/s are marked in yellow.

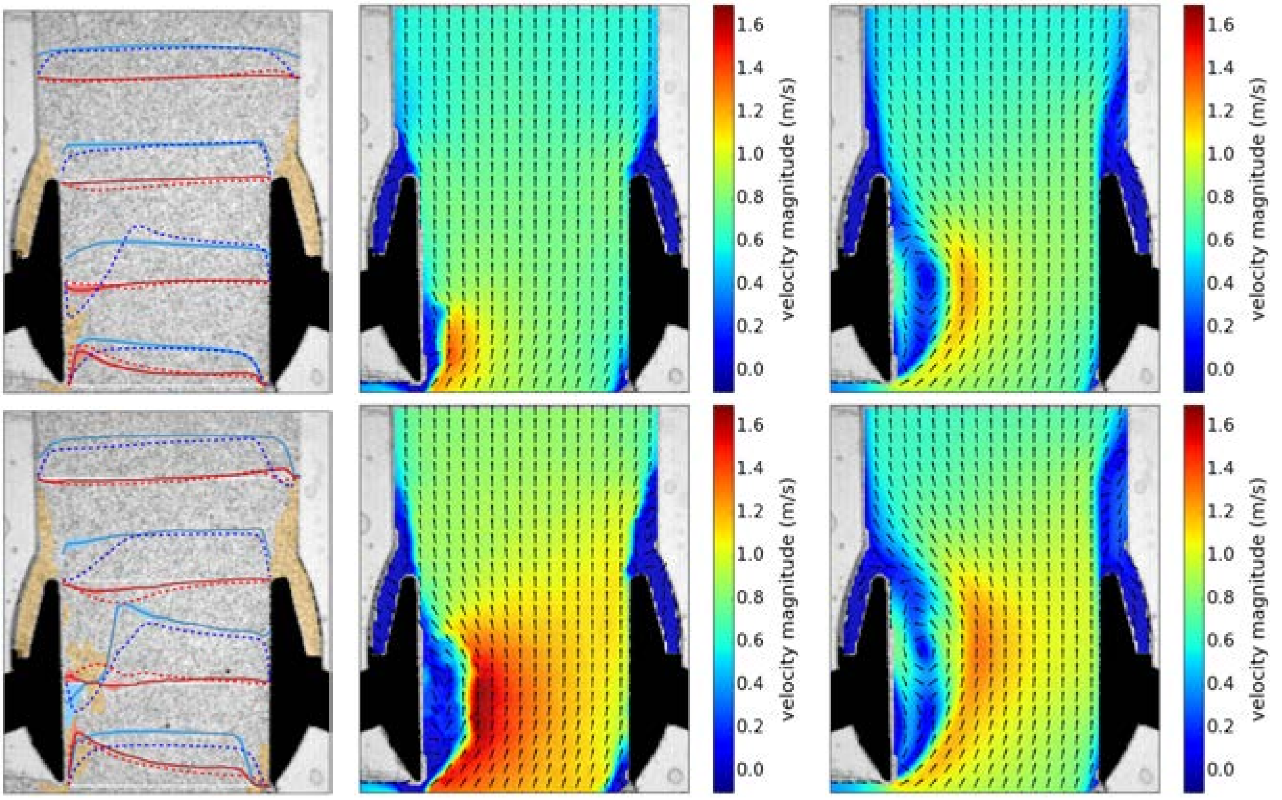

Figure 5: Left column: PIV and CFD velocity profiles for Case 4 at 0.08 and 0.1 sec, respectively. **Middle column:** PIV velocity vectors for Case 4 at 0.08 and 0.1 sec, respectively. **Right column:** CFD velocity vectors for Case 4 at 0.08 and 0.1 sec, respectively. The PIV velocity vector plot at 0.08sec (1st row and 2nd column) shows that a wake is forming at the left coronary leaflet. The CFD velocity profile at 0.08sec (1st row and 3nd column) shows that a large wake is already present in the CFD simulation. Additionally, the PIV velocity vector plot at 0.1sec shows (2st row and 2nd column) show that the PIV analysis is not able to pick up the detailed flow field in the wake at the left coronary leaflet where the velocities are small

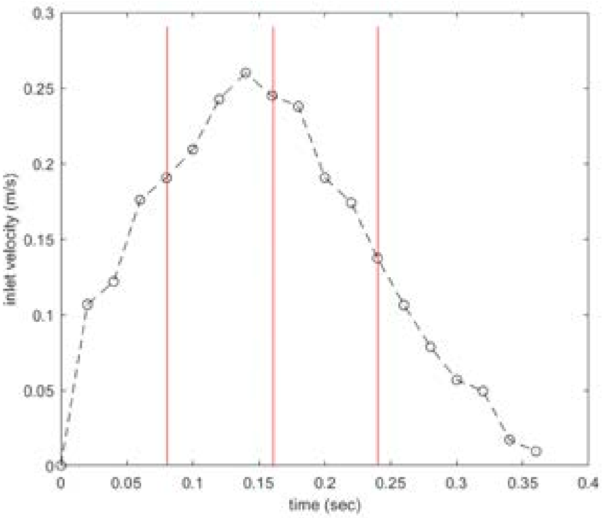

Figure 3: The inlet flow velocity derived from the volume change between successive frames in a patient specific ultrasound recording. The volume curve at the top of Figure 4 represents the accumulated ejection volume and is thus smoother than the velocity curve. The vertical red lines indicate the times visualized in Figure 4.

Table 2. In Figure 4, the top row shows illustrations of the geometry of the LVOT for the four cases, where the removable inserts are colored orange. The inflow waveform used in the experimenters is given in the left column of Figure 4 and 3. The curves in Figure 4 shows remaining ejection volume of the ventricle as a function of time and defines the volume flow in the loop, Figure 3 shows the corresponding development in inlet velocity. The systole begins at time zero and ends at 0.360 sec. Velocity profiles at three times and four different positions in the aortic valve apparatus during systole is given in the figure, at 0.08, 0.16 and 0.24 sec. The blue velocity profiles give the velocity components in the axial direction (y-direction) and the red velocity profiles give the velocity components in the transverse direction (x-direction). The PIV results from the in-vitro flow loop is given by solid lines, and is averaged over six cardiac cycles. Additionally, at the three selected times, velocities are averaged in a time span of 3 milliseconds (i.e. 3 PIV frames). The plotted blue and red areas give the standard deviation in the PIV data. The velocity profiles components from the CFD calculations are given by blue and red dashed lines, for the axial and transverse direction respectively.

Velocity profiles for Case 1, where there is no AML billowing nor ASH bulging, remains relatively flat throughout systole, as can be seen in Figure 4.There is however a recirculation zone adjacent to the left coronary leaflet. The recirculation zone develops during systole due to the angle between the anterior mitral leaflet and the left coronary leaflet. For Case 2, with an ASH bulging of 9mm, a small re-circulation zone can be seen at the root of the right coronary leaflet. The re-circulation zone does not extend into the aorta and is caused by the angle between the ASH bulging right coronary leaflet. A 9 mm AML billowing, as defined in Case 3, causes a larger recirculation zone adjacent to the left coronary leaflet

Table 2: Maximum axial velocities for the velocity profiles (blue solid lines) given in Figure 4, at flow times 0.08, 0.16 and 0.24 seconds, for Case 1, 2, 3 and 4. At each flow time, four velocity profiles are plotted at regular increments in the vertical direction starting at the root of the aortic vales, as seen in Figure 4. The maximum velocities given in the table are arranged in the same vertical order as the velocity profiles in Figure 4.

Time [s]	Case 1 [m/s]	Case 2 [m/s]	Case 3 [m/s]	Case 4 [m/s]
0.08	0.57	0.61	0.69	0.68
	0.70	0.71	0.85	0.82
	0.67	0.79	0.84	0.88
	0.85	1.03	0.90	0.99
0.16	0.92	0.99	1.00	1.27
	0.92	1.10	1.09	1.34
	1.03	1.17	1.11	1.24
	0.87	0.94	0.86	0.92
0.24	0.78	0.94	0.99	1.31
	0.74	1.03	1.04	1.19
	0.87	0.95	0.91	0.97
	0.66	0.81	0.74	0.80

compared to the physiological case (Case 1). However, the axial velocity profiles remains relatively flat throughout the systole, and there are little cross flow in the transverse direction. Large re-circulations zones adjacent to the left coronary leaflet were found for Case 3 and Case 4. They are indicated as areas shadowed by yellow color in Figure 4. These areas were discriminated by having a velocity magnitude smaller that 0.1 m/s. There is also significant back flow downstream of the left coronary leaflet in the ascending aorta. Case 4 has the highest presence of transverse flow through the aortic vales and also exhibits a re-circulation zone similar to that of Case 2 at the root of the right coronary leaflet.

The PIV velocity vector plot at 0.08 sec (Figure 5, top left panel) shows that a wake is forming at the left coronary leaflet. The CFD velocity profile shows that a large wake is already present in the CFD simulation at 0.08 sec. Additionally, the PIV velocity vector plot at 0.1 sec shows (Figure 5, top left panel) show that the PIV analysis is not able to pick up the detailed flow filed in the wake at the left coronary leaflet where the velocities are small.

DISCUSSION

In this work, we performed both in-vitro experiments and CFD calculations on the 2D LVOT model. The 2D models were parametrized according to Table 1, where Case 1 represents the normal physiological geometry. AML billowing was simulated by removing a 9mm wide insert (Case 2, Table 1) in the mitral valve position, as seen in Figure 1. ASH was simulated by inserting a 9mm wide insert (Case 3, Table 1) on the right LVOT wall, as seen in Figure 1. Finally, both AML billowing and ASH was simulated in Case 4.

The agreement between the PIV results and the CFD calculations can be seen in Figure 4 and 5. The largest discrepancy between the experimental data and the numerical results can be seen in the re-circulation zone adjacent to the left coronary leaflet. The timing of the development of the circulations zone is not exactly the same for the CFD and the experimental results. From the axial velocities one can observe that there is some time shift between the experimental and the CFD results. The most likely cause of this time lag originate from some compliance present in the experimental setup which delays the flow wave form into the LVOT compared to the CFD results, as seen in Figure 5. Moreover, the current PIV setup was not able to map the small velocities in the re-circulation zone at the left coronary leaflet as seen in Figure 4 and 5, this was also confirmed by testing an alternative PIV software (PIVlab). The velocity field in the recirculation zone can determined by analyzing this region with higher spatial resolution, i.e. smaller polymer particles and increased camera resolution/zoom.

Flow velocity measurements based on particle shadows allows for low-power illumination compared to a conventional laser PIV setup. Additionally, since the light source in shadow PIV can illuminate continuously, the temporal resolution is only restricted by the frame rate of the high-speed camera and not on a laser system. A drawback with the shadow PIV technique is that it is not possible to isolate particles in a specific plane in the depth direction of the flow domain (i.e. in the line defined by the camera an the light source), which is the strong point of laser PIV where typically a laser sheet is used to illuminate particles in a specific 2D plane (Estevadeordal and Goss, 2005). However, by adjusting the focus point of the camera in the center of the flow domain (in the depth direction) we were to some extent able to favorize particles in the center plane of the flow model. A second issue with shadow PIV technique in the current setup is the particle size. As shown in Sec. *Experimental setup*, the particles in our setup have a Stokes number in the order of 0.75, which is somewhat high for following the flow as true tracers. A smaller Stokes number could be achieved in our setup with a high speed camera with higher resolution, which will be considered for future studies.

The main limitations in the current study when evaluating the clinical significance of the results are the choice of a 2D geometry with stiff and stationary walls. The 2D geometry will introduce unnatural flow conditions compared to the real 3D case, such as increased vortex formation. Moreover, the aortic valves are not to allowed to move in our current flow model. In the real physiologic case, the aortic vale leaflets are highly deformable structures and the final fully open position during systole is believed to be significantly influenced by the local flow conditions in the LVOT. A more realistic in-vitro setup for future studies might involve a full 3D geometry with a biological prosthetic aortic vale.

CONCLUSION

In conclusion, while keeping in mind the limitations of the current study from a clinical perspective as discussed above, our results show that ASH bulging alone does not alter the flow field in the LVOT dramatically. However, for AML billowing and for the combination of AML billowing and ASH, we see a significant re-circulation zone covering half of the aortic outflow tract at peek systole (i.e. 160ms into the cardiac cycle), as seen in e.g. Case 4 in Figure 4. This result is not surprising since these two cases produce large expansion angles between the LVOT and the aortic outflow tract. Which in turn, might cause asymmetrical hemodynamical loads on the aortic valve leaflets and downstream compactions.

REFERENCES

DAHL, S.K. (2012). *Numerical simulations of blood flow in the left side of the heart*. Ph.D. thesis.

DAHL, S.K., FAGERHOLT, E., KISS, G., PROT, V.E., AMUNDSEN, B.H., HELLEVIK, L.R. and SKALLERUD, B.H. (2011). "3d moving boundary conditions for heart cfd simulations - from echocardiographic recordings to discretized surfaces". *MekIT'11: Sixth National Conference on Computational Mechanics*, 33–46. Tapir Akademisk Forlag.

DIMASI, A., CATTARINUZZI, E., STEVANELLA, M., CONTI, C.A., VOTTA, E., MAFFESSANTI, F., INGELS JR, N.B. and REDAELLI, A. (2012). "Influence of mitral valve anterior leaflet in vivo shape on left ventricular ejection". *Cardiovascular Engineering and Technology*, **3(4)**, 388–401.

ESTEVADEORDAL, J. and GOSS, L. (2005). "An investigation of particle-shadow velocimetry (psv) for transonic-flow applications". *35th AIAA Fluid Dynamics Conference and Exhibit*, 5009.

ISRAEL, R. and ROSNER, D.E. (1982). "Use of a generalized stokes number to determine the aerodynamic capture efficiency of non-stokesian particles from a compressible gas flow". *Aerosol Science and Technology*, **2(1)**, 45–51.

KUPARI, M. and KOSKINEN, P. (1993). "Systolic flow velocity profile in the left ventricular outflow tract in persons free of heart disease". *The American journal of cardiology*, **72(15)**, 1172–1178.

KVITTING, J.P.E., BOTHE, W., GÖKTEPE, S., RAUSCH, M.K., SWANSON, J.C., KUHL, E., INGELS, N.B. and MILLER, D.C. (2010). "Anterior mitral leaflet curvature during the cardiac cycle in the normal ovine heartclinical perspective". *Circulation*, **122(17)**, 1683–1689.

MATRE, K., KVITTING, P., ZHOU, Y. and FAERESTRAND, S. (2003). "The effect of body weight on the degree of blood velocity profile skewness in the aortic annulus in domestic pigs". *Laboratory animals*, **37(1)**, 72–80.

SJÖBERG, B.J., ASK, P., LOYD, D. and WRANNE, B. (1994). "Subaortic flow profiles in aortic valve disease: a two-dimensional color doppler study". *Journal of the American Society of Echocardiography*, **7(3)**, 276–285.

TAYLOR, Z.J., GURKA, R., KOPP, G.A. and LIBERZON, A. (2010). "Long-duration time-resolved piv to study unsteady aerodynamics". *IEEE Transactions on Instrumentation and Measurement*, **59(12)**, 3262–3269.

TROPEA, C., YARIN, A.L. and FOSS, J.F. (2007). *Springer handbook of experimental fluid mechanics*, vol. 1. Springer Science & Business Media.

XIONG, F., YEO, J.H., CHONG, C.K., CHUA, Y.L., LIM, K.H., OOI, E.T. and GOETZ, W.A. (2008). "Transection of anterior mitral basal stay chords alters left ventricular outflow dynamics and wall shear stress". *Journal of Heart Valve Disease*, **17(1)**, 54.

YOUSIF, M.Y., HOLDSWORTH, D.W. and POEPPING, T.L. (2011). "A blood-mimicking fluid for particle image velocimetry with silicone vascular models". *Experiments in fluids*, **50(3)**, 769–774.

ZHOU, Y., FAERESTRAND, S., MATRE, K. and BIRKELAND, S. (1993). "Velocity distributions in the left ventricular outflow tract and the aortic anulus measured with doppler colour flow mapping in normal subjects". *European heart journal*, **14(9)**, 1179–1188.